Degradation of Phenol With A Microwave-Uv Irradiation Treatment System Using NANO-TiO_2

Abha Verma, Venkatesh Meda*, Sandeep Badoga and Ajay Dalai

Chemical and Biological Engineering, University of Saskatchewan, Saskatoon, SK, S7N 5A9, Canada

Abstract: The degradation of phenol from various industrial effluents becomes essential and studied in this work. The microwave (MW), ultra-violet (UV) and combination treatment systems were designed and TiO_2 nanoparticles were used as photocatalyst for the degradation of 1500ppm phenol in a solution. It was observed that the degradation efficiency was less than 10% in both MW and MW-UV systems without a catalyst. However, the addition of TiO_2 particles in MW-UV system has increased the phenol degradation efficiency significantly. The extent of increase in degradation efficiency is dependent on the structural and optical characteristics of TiO_2, which is affected by the TiO_2 preparation method. In this work, the TiO2 nanoparticles with anatase structure were synthesized by hydrothermal (HT) and sol-gel (SG) methods. The synthesized materials were characterized using X-ray diffraction, FT-IR, thermogravimetric analysis, SEM, high resolution TEM and BET method. The higher degradation efficiency of 24% shown by MW-UV-TiO_2 (HT) system in 120 minutes as compared to 20% shown by MW-UV-TiO_2 (SG) system could be due to higher surface area and better textural properties of TiO_2 prepared by hydrothermal treatment. The effect of various initial concentration of phenol (500-1500ppm) on degradation efficiency of MW-UV-TiO_2 (HT) system revealed that the increase in the initial phenol concentration decreased the phenol degradation efficiency.

Keywords: Phenol-water, dielectric properties, microwave, hydrothermal TiO_2, Sol-Gel TiO_2, Nano-TiO_2.

1. INTRODUCTION

The rapid growth of industries are creating more stress on the environment to deal with the wastes generated. Phenol is one of the many pollutants, discharged from various industries including; paper milling, olive oil extraction, textiles and resin manufacturing, wood processing, coal gasification, oil refining and agro-industrial wastes [3, 10]. Presence of phenol in portable water can cause diarrhea, severe effect on the kidneys and central nervous system [11]. Its concentration higher than 2 mg L^{-1} is toxic to fish and other aquatic life. Therefore, considering the harmful effects of phenol, it is listed as priority pollutant by the US Environmental Protection agency (EPA) [29].

Alberta, Canada has one of the largest facilities to process oil sands in the world. The oil extraction process requires a huge quantity of water. Approximately 3 barrels of fresh water is required to produce one barrel of oil from oil sands and the waste water is sent to the tailing ponds. The waste water contains many organic pollutants such as bitumen, naphthenic acids, asphaltenes, benzene, creosols, humic and fulvic acids, phenols, phthalates, polycyclic aromatic, hydrocarbons, and toluene [23, 19, 13, 18, 32, 42]. Typical concentration of phenolic compounds in oil sands process water is less than 55 mg/L [54]. With increasing oil production the size of tailing ponds is increasing and now it is a big challenge to treat the tailing ponds before the waste water can be recycled or discharged to the environment. With this need, various methods such as photocatalytic degradation [22, 16], advanced oxidation processes (AOPs) such as ultra violet (UV), UV-H_2O_2, ozone (O_3) and UV-O_3 [2,35,38] have become popular in recent years as efficient treatment methods for degrading compounds like phenol and its derivatives [39, 47, 6]. However, the microwave assisted advanced oxidation processes are proven to be the most promising technology for the degradation of phenol and has been used for a large variety of organic pollutants like polycyclic aromatic hydrocarbon (PAHs) and polychlorinated biphenyls (PCBs) [45, 7, 46]. The stringent environmental regulations are pushing researchers to innovate such methods which can improve the efficiency of degradation of pollutants in waste water treatment process. In this effort, recently the combination of catalytic oxidation with microwave and UV irradiation were tested. Various materials such as ZnO, TiO_2, ZnS, CdS, Fe_2O_3, TiO_2 doped with CuO and alumina, have been used as a catalyst due to their photocatalytic properties.

Microwave energy has widely been applied in domestic, industrial and medical fields during the past two decades. It has been found that microwave irradiation not only can excite an electrodeless discharge lamp (MWL) to generate ultraviolet (UV) radiation which can excite TiO_2 for photocatalysis, but also could significantly improve the photocatalytic activity of TiO_2 for removing pollutants [53]. Using

*Address correspondence to this author at the 57 Campus Drive, Saskatoon SK Canada, S7N5A9, Canada; Tel: 1-306-966-5309;
E-mail: vem281@campus.usask.ca

E-ISSN: 2410-3624/17

microwave irradiation rather than conventional heating has improved product selectivity and accelerated reaction rates [48, 49, 38]. It has been found that in the presence of microwave irradiation the photocatalytic efficiency of TiO_2 to remove pollutants was increased significantly [36]. The betterment of photocatalytic activity was because of the polarization effect of the highly defected catalysts in a microwave field, which increased transition probability of photon-generated electrons and decreased the electron–hole recombination on semiconductor surface [4]. Horikoshi *et al*. [36] illustrated that the synergistic effect of UV and microwave radiation in the presence of TiO_2 was superior for the degradation of rhodamine-B dye to TiO_2 photocatalytic degradation alone with UV radiation.

Titanium dioxide (TiO_2) is a white, solid, inorganic substance that is thermally stable, non- flammable and not classified as hazardous material [50]. Among the various semiconductor materials, it is the most widely used photocatalyst due to its non-toxicity, high activity, high stability, and low cost. It can generate highly reactive oxygen species such as O^{2-} and $HO^{\bullet}$, responsible for the oxidation of a wide variety of aliphatic and aromatic hydrocarbons [9].

Nanosized TiO_2 has received much interest for applications such as optical devices and sensors, and photocatalysis has been used for environmental decontamination of a variety of organic compounds [12]. The photocatalytic activity of titanium nanoparticles varies depending on its crystallinity, particle size, crystal phase, surface area, method of preparation, porosity, and shape and size distribution of pores [44, 40]. TiO_2 exists in three forms and the band gap changes with a change in the phase from anatase (3.2 eV) to rutile (3.02 eV) to brookite (2.96 eV). It is known that the anatase form with small particle size and high crystallinity is required to obtain highly active titanium photocatalysts. The higher photodecomposition activity shown by anatase phase of TiO_2 is due to its large band gap [1,43]. Chhabra *et al*. [41] has also shown that only anatase TiO_2 particles act as a photocatalyst for the photodegradation of phenol, and that the rutile form is totally inactive for this reaction.

Photocatalytic oxidation reactions are initiated when a photon of higher energy level or equal to the band gap energy is absorbed by a TiO_2 catalyst promoting an electron transfer (e^-) from the valence band to the conduction band with simultaneous generation of a positive hole (h^+) in the valence band [38]. The mechanism of radical generation ($^{\bullet}OH$ and $^{\bullet}O2^-$) is presented as follows [26]:

$$TiO_2 + h\nu \rightarrow TiO_2\left(e + h^+\right) \quad (1)$$

$$H_2O + TiO_2\left(h+\right) \rightarrow TiO_2 + {}^{\bullet}OH + H^+ \quad (2)$$

$$O_2 + TiO_2\left(e^-\right) \rightarrow TiO_2 + {}^{\bullet}O_2^- \quad (3)$$

In the present work, TiO_2 nanoparticles were synthesized using two methods; hydrothermal and sol-gel methods. These methods provide excellent chemical homogeneity and the possibility of deriving unique metastable structures. It involves the formation of a metal-oxo-polymer network from molecular precursors like metal alkoxides or metal salts. For example, the metal alkoxides may be hydrolyzed (eq. 4) and polycondensed (eq. 5 and 6) to form a metal oxide gel as follows:

$$M-OR + H_2O \rightarrow M-OH + ROH \quad (4)$$

$$M-OH + M-OR \rightarrow M-O-M + ROH \quad (5)$$

$$M-OH + M-OH \rightarrow M-O-M + H_2O \quad (6)$$

where, M is Si, Ti, Zr, Al, etc. and R is an alkyl group. The structure and properties of the resulting metal oxides are strongly influenced by relative rates of hydrolysis and polycondensation [25].

Several attempts have been made previously to synthesize TiO_2 nanoparticles *via* hydrothermal and sol-gel routes [8, 21] but their photocatalytic activity using microwave and microwave combined ultraviolet radiation has not been explored thoroughly. It is interesting to compare the catalyst's physiochemical (surface area, particle size) and photocatalytic properties if prepared with the same precursors, solvents and calcined at same temperature.

Therefore, the objective of this work was to determine and compare the efficiency for degradation of phenol by using two catalysts (prepared *via* two different methods) in two laboratory scale systems: (i) microwave only, and (ii) microwave assisted UV treatment. The TiO_2 catalysts were characterized using N_2 adsorption-desorption, X-ray diffraction, FT-IR, SEM and TEM.

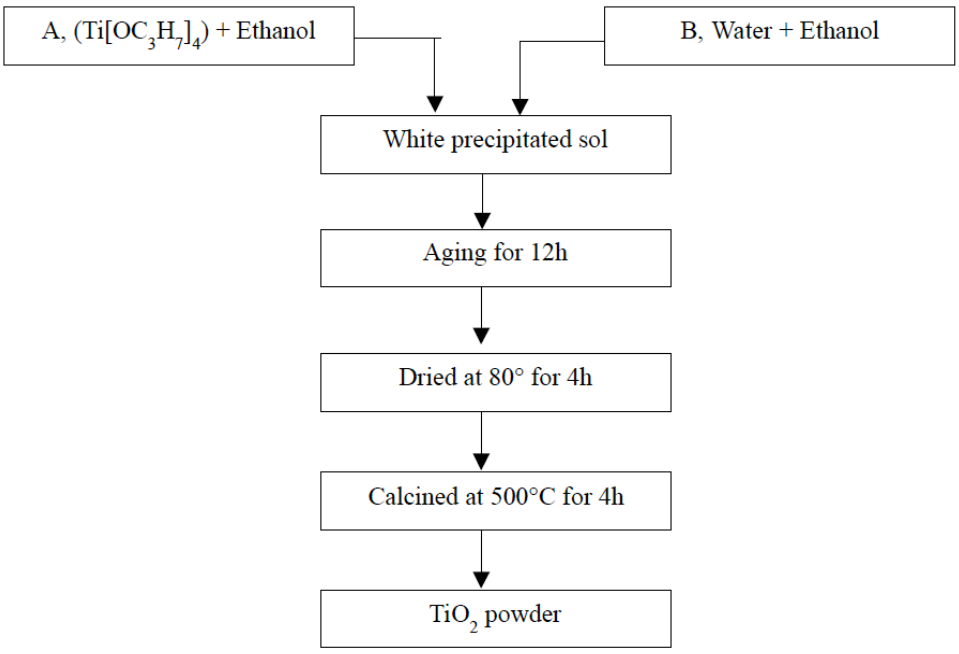

Figure 1: Schematic diagram for the synthesis of TiO_2 powder by a sol-gel method.

2. MATERIALS AND METHODS

2.1. Chemicals

Analytical grade reagents were used in the synthesis without further purification. Titanium (IV) isopropoxide (Ti $[OC_3H_7]_4$ TTIP) and anhydrous ethanol were purchased from Alfa Aesar, Edmonton, CA. Phenol was obtained from Sigma Chemical Co. (St. Louis, MO, USA) and a stock solution of 2000 ppm phenol in water was prepared. All solutions were prepared using Milli-Q water from an EASY-pure ultrapure water system.

2.2. Synthesis of TiO_2 by the Sol-Gel Route

TiO_2 nanoparticles were synthesized by hydrolyzing titanium tetra isopropoxide (TTIP) in a mixture of anhydrous ethanol and water as shown in Figure **1**. Two solutions were made: A, TTIP mixed with

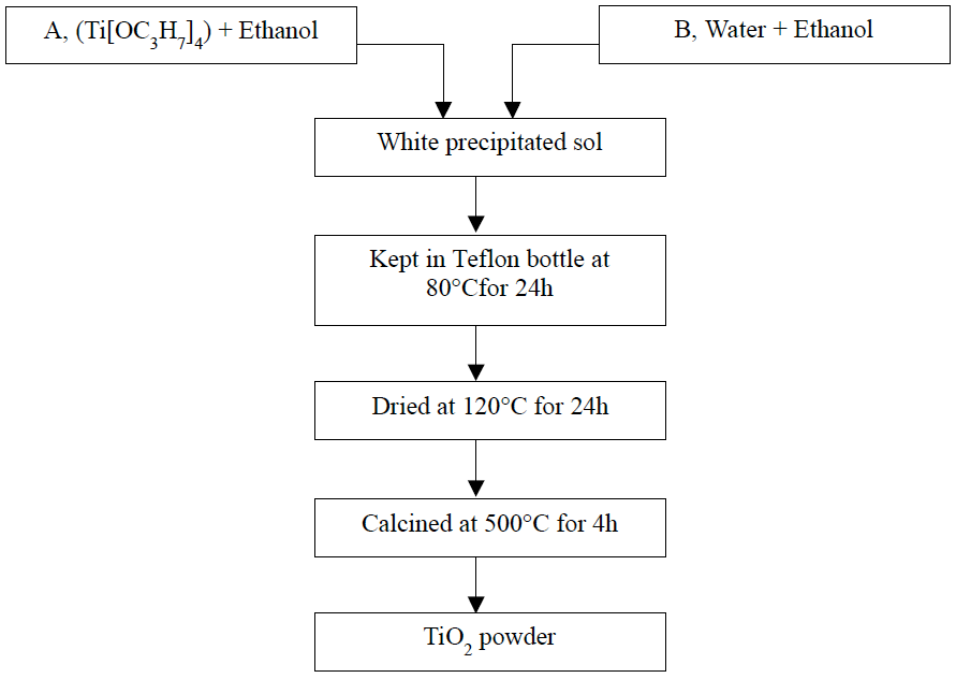

Figure 2: Schematic diagram for the synthesis of TiO2 powder by a hydrothermal method.

anhydrous ethanol, and B, water mixed with ethanol. Solution A was added dropwise to solution B with constant and vigorous stirring for 2 h. Hydrolysis and condensation were conducted at room temperature and underwent aging for 12 h. The gel was dried in an oven at 80°C for 4h; it was then crushed into fine powders with a mortar and pestle and then calcined at 500°C [20]. The obtained material is named as TiO_2 (SG).

2.3. Synthesis of TiO_2 by the Hydrothermal Method

A schematic diagram for the synthesis of TiO_2 powder by the hydrothermal method is shown in Figure **2**. After 2 h stirring, the solution was transferred in to a Teflon bottle and placed in an oven at 80°C for 24 h. The resulting solution was filtered and dried at 120°C for 24 h, then crushed into a fine powder with a mortar and pestle and calcined at 500°C for 4 h to produce TiO2 powder (TiO_2 (HT) [20].

2.4. Catalyst Characterization Methods

2.4.1. X-Ray Diffraction (XRD) Analysis

Phase analysis of calcined TiO_2 powder was carried out using a Bruker D8 Series II Advance X-ray powder diffractometer using Cu Kα radiation. The specimen was mounted in the center of the diffractometer and rotated by angle (θ) [33]. The wide-angle scan was made from 10 to 90° with 2θ step size of 0.1.

2.4.2. Measurement of N_2 Adsorption–Desorption Isotherms

The surface area and pore size distribution of the prepared catalyst *via* two different methods were measured with Brunauer–Emmett–Teller (BET) and Barrett-Joyner-Halenda (BJH) method using a Micromeritics ASAP 2020 instrument. The sample was degassed in vacuum at 300°C before measurement. The surface area was computed using the multi-point Brunauer-Emmett-Teller (BET) method from isotherms. The BJH method was used to determine pore diameter and pore volume [34].

2.4.3. Fourier Transform Infrared Spectroscopy (FTIR)

Fourier transform infrared (FTIR) spectra of the samples were obtained in the spectral range of 400-4000 cm^{-1} at a resolution of 4 cm^{-1} (Perkin-Elmer Spectrum GX). KBr pellet technique was used to obtain infrared spectra of the prepared catalysts at room temperature [33].

2.4.4. Scanning Electron Microscopy (SEM) and HIGH Resolution Transmission Electron Microscopy (HRTEM)

Morphological analysis was carried out using a field-emission scanning electron microscope (JSM–6010L V) operating at 20 keV and HRTEM images were obtained using a JEOL 2011 scanning transmission electron microscope.

2.4.5. Thermogravimetric Analysis (TGA)

The thermal stability of the oxides was studied by thermogravimetric analysis (TGA Instruments model TGA-Q500). 0.04g of sample was heated from 25 to 800°C in flow of nitrogen (30 ml/min) with a heating rate of 10°C/min.

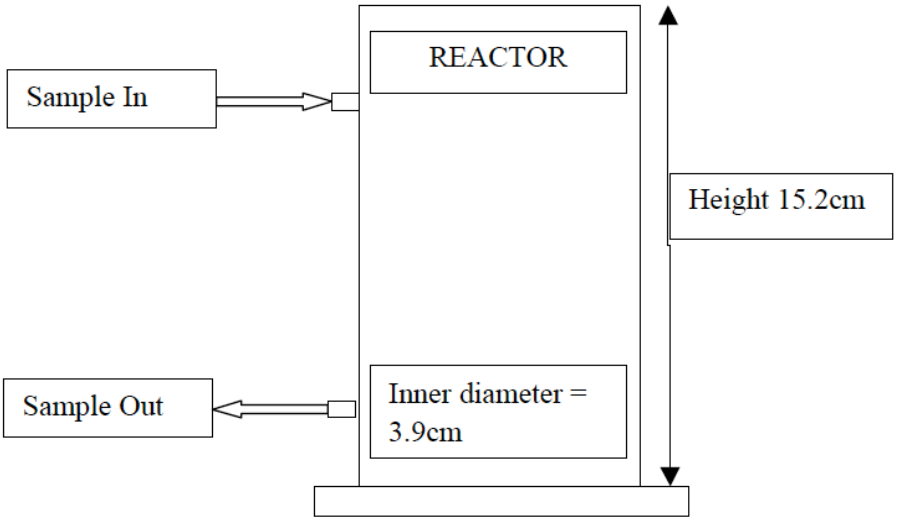

Figure 3: Schematic of Teflon Reactor used in MW-UV Reactor.

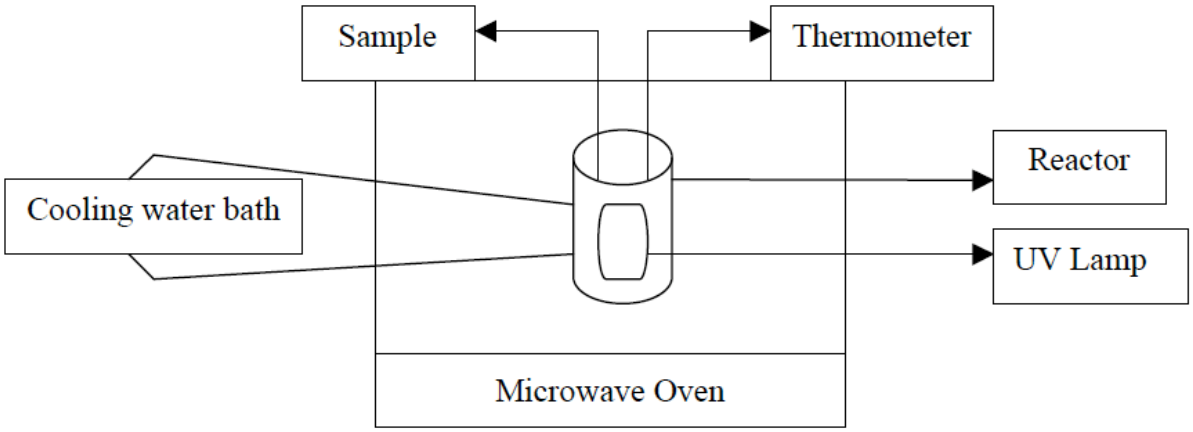

Figure 4: Schematic of combined microwave-UV treatment system.

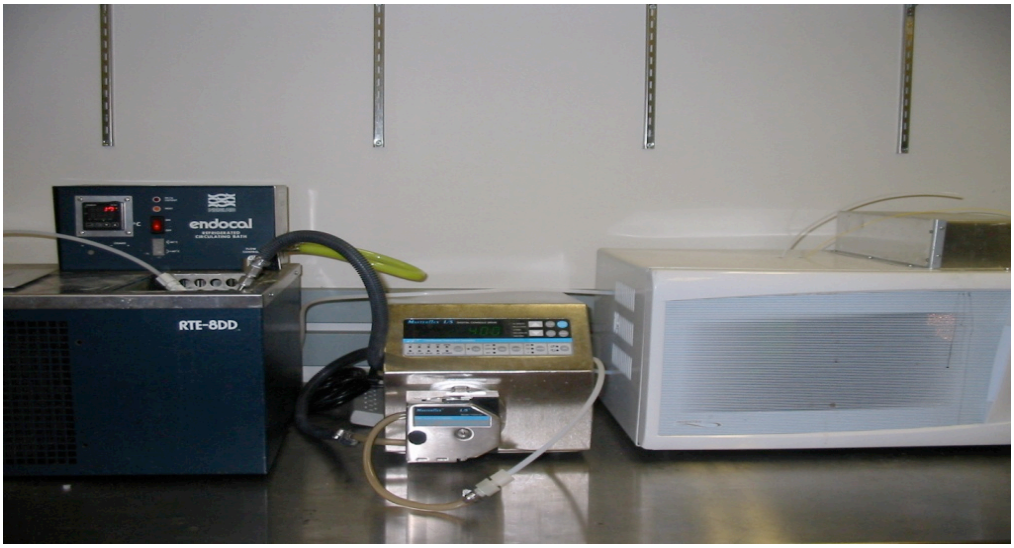

Figure 5: Photograph of the experimental setup.

2.5. Experimental Setup for the MW-UV Treatment System

Microwave experiments were performed using a household microwave (NNS615W, 1200 W, 2.45 GHz, Panasonic Canada Inc., Mississauga, ON) which was modified to accommodate the reaction chamber/ sample holder and tubing made of Teflon (see Figure **3**). The sample holder was designed and fabricated in the Engineering Shops of the University of Saskatchewan, (Saskatoon, SK). A schematic of the experimental set up is shown in Figure **4** and a photographic view is presented in Figure **5**.

To make a combined microwave-UV treatment system, a microwave electrodeless lamp (λ_{max} = 254 nm, power intensity 8W) placed centrally inside the reaction chamber was used as the source of ultraviolet (UV-254) rays (Figure **6**).

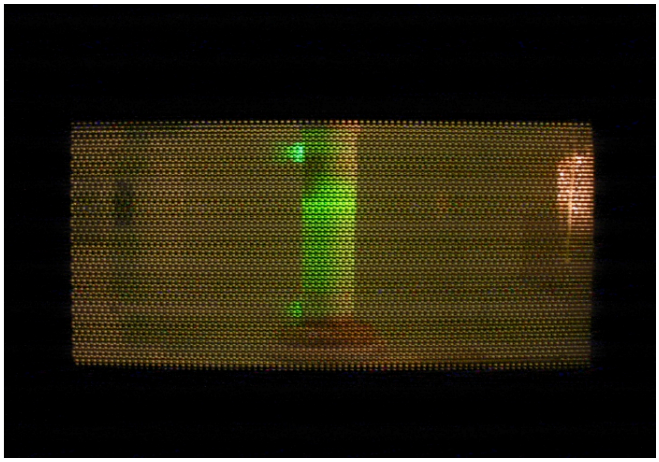

Figure 6: Photograph of the microwave electrodeless lamp inside the reactor.

This lamp was custom built and produced by Primarc UV Tech. (Easton, PA). Details on the working principle of this lamp are available in the literature [28].

Microwave is absorbed by the electrodeless lamp which in turn emits the necessary UV rays for photocatalysis. An electrodeless lamp was used in this system because an electrode UV lamp in a microwave oven is not only difficult, but also unsafe because the lamp can be damaged by the electric discharge between the microwave oven and the metallic part of the lamp [36]. The turntable glass plate in the microwave oven was removed to stop rotation of the reactor and to avoid damage to the reactor and electrode less lamp. A round teflon plate was designed with the same circumference as the teflon reactor for the mercury lamp to stand vertical. Two holes were drilled at the top surface of the microwave, one was to take samples and the other was to insert the fiber optic temperature probe. Two holes were made in the side wall of microwave as well, the lower one was to get the sample out to the water bath and the upper one was for sample to recycle back to the reactor after cooling. In this system, a 300 mL sample of 1500 ppm phenol concentration was mixed with 1 g of TiO_2 at 40°C. The circulation through chiller/water bath was done with a flow rate of 400 mL/min for 120 min. No attempt was made to adjust the pH of the phenol-water solution. The degradation of phenol in the presence of catalyst was studied.

A peristaltic pump was used to circulate the phenol-water mixture from the reaction chamber closed system through a cooling coil. In this way the temperature of the sample could be maintained at 40°C. This also allowed the mixture to have sufficient residence time to stay inside the reaction chamber for maximum possible exposure to microwave radiation. The dosage of TiO_2 has been presented in the methodology flow chart (Figure **7**). Samples were collected every 20 min. Experiments were replicated three times at each level.

2.6. Analytical Methods

1-2 ml samples were taken with a 10 mL syringe from the reactor at different pre-determined reaction times. The collected photocatalysis samples were first filtered through a 20 µm nylon filter to remove the TiO_2 particles prior to chemical analysis. All the samples were analyzed immediately to avoid any further reaction. The concentration of phenol was quantified by HPLC. A 20 µL sample was injected into the D-7000 HPLC system (Hitachi, Japan) equipped with a C18 column (Hypersil, China. 250×4.6 mm), which consisted of a L-7100 pump and a L-7420 UV-VIS detector. A 60% (v/v) aqueous acetonitrile solution and 40% water was used as the mobile phase; its flow rate

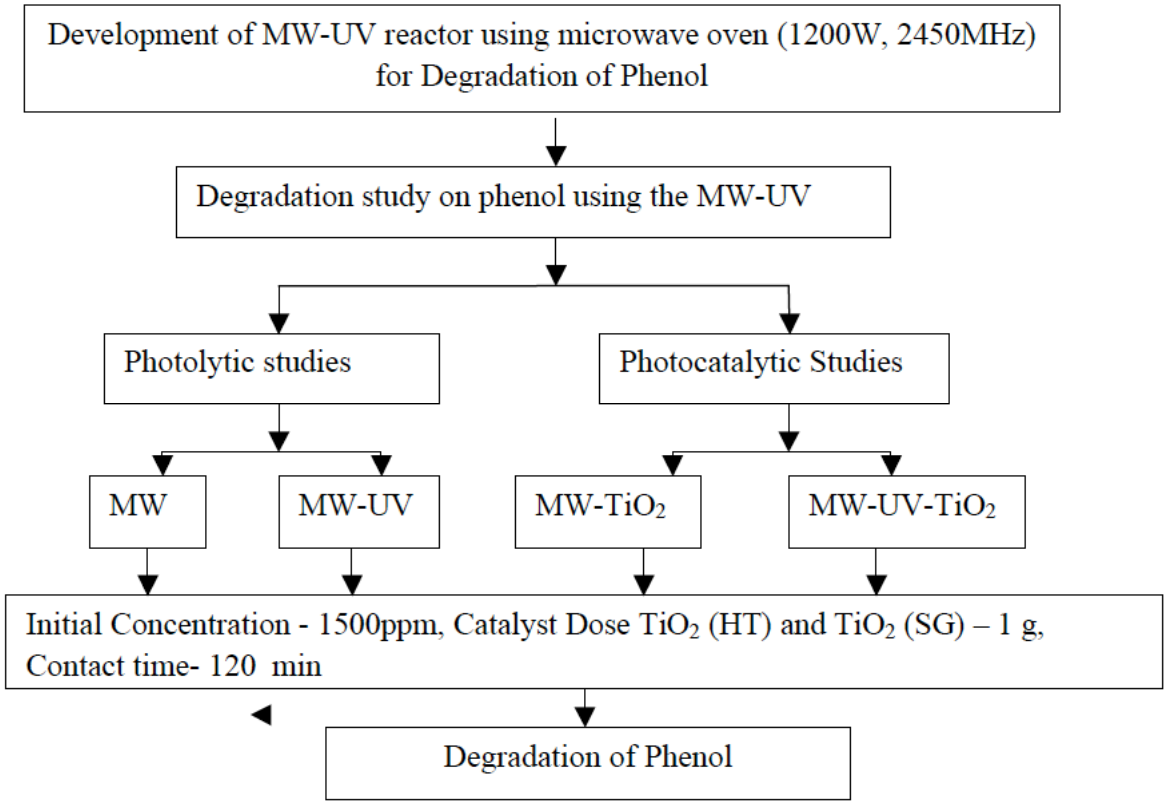

Figure 7: Flow chart of the methods followed in experiments using the initial concentration 1500 ppm of phenol for 120 min with 1 g of catalyst prepared by hydrothermal and sol-gel methods.

was fixed at 1 mL/min. The wavelength employed for detecting phenol was 254 nm.

2.7. Experimental Methodology

The phenol-water solution (1500 ppm) solutions was prepared by dissolving pure phenol in Milli - Q water and stored in amber-colored bottles. A total of 300 mL of the phenol-water solution was added to a batch reactor with the catalyst concentration as explained in the experimental methodology flow chart (Figure **7**).

The mixture of phenol-water and catalyst was homogenized with a magnetic stirrer before placing in the sample holder inside the microwave. The solution was circulated at 400 mL/min with a pump, and the temperature of phenol-water solution in the reactor vessel was kept constant at 40°C.

3. RESULTS AND DISCUSSION

3.1. Characterization of the TiO_2 Nanoparticles

3.1.1. X-ray Diffraction (XRD)

The structure and the crystallite size of the prepared samples were examined by wide angle X-ray diffraction analysis. Figure **8** presents the XRD patterns of calcined TiO_2 nanopowder prepared by two different methods and calcined at 500°C. The peaks obtained at various 2θ were identified by comparison with ICDD (International Centre for Diffraction Data) which confirmed that the particles were crystalline with an anatase structure (2θ = 25, 37.8, 48.0, 54.0, 55.1, 62.7, 68.8, 70.2, 75.2 and 82.4) [51]. They were assigned to the 101, 004, 200, 105, 211, 204, 116, 220, 215 and 312 diffraction peaks of anatase TiO_2.The absence of peaks at Bragg angles (2*θ*) of 27.5°, 39.3°, and 54.2° confirmed the absence of the rutile phase in the samples. The anatase form is more catalytically active as compared to rutile phase. Therefore, the material synthesized is expected to show catalytic activity. The average crystallite size of TiO_2 was estimated according to Scherrer's equation (equation 8).

$$D = K\lambda / \beta \text{Cos}\theta \quad (8)$$

where, K is the Scherer constant (0.9), λ the X-ray wavelength (1.54nm), β the peak width at half maximum, and θ is the Bragg diffraction angle. It has been found that the crystallite size of TiO_2 nanoparticle synthesized with hydrothermal method is ~17nm whereas with sol-gel method it is ~19nm.

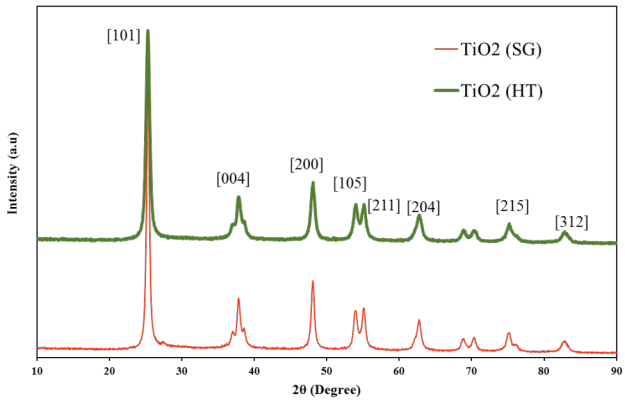

Figure 8: X-ray diffraction (XRD) patterns of TiO_2 prepared by sol-gel (SG) and hydrothermal (HT) methods.

3.1.2. N_2 Adsorption – Desorption Isotherm

Nitrogen sorption at 77 K using a micromeritics ASAP 2020 instrument was used to measure the textural properties of the catalysts. The BET method was used for the determination of the surface area and pore volume of the samples using adsorption-desorption isotherms [33]. The pore diameter and pore size distribution of the catalysts were determined using the BJH method. They are summarized in Table **1** which shows a higher surface area of the catalyst prepared by the hydrothermal process (HT) (85 m^2/g) as compared to that prepared by the sol-gel method (SG) (36 m^2/g). However, the average pore diameter of the catalyst prepared by the hydrothermal method was smaller than that of the sol-gel prepared catalyst, 10.4 nm and 15.7 nm respectively. Also, the pore volumes of TiO_2 prepared by HT method is two times that of TiO_2 prepared by SG method. The BET analysis has confirmed that the material TiO_2 (HT) has superior textural properties as compared to material TiO_2 (SG).

Table 1: Summary of the Properties of TiO_2 Nanoparticles Calcinite at 500°C

Properties	TiO_2 (HT)	TiO_2 (SG)
Surface area (m^2/g)	85	36
Avg. pore diameter (nm)	10	15
Pore Volume (cm^3/g)	0.2	0.1

3.1.3. Thermogravimetric Analysis (TGA)

Figure **9** presents TGA curves for as synthesized TiO_2 by sol-gel and hydrothermal methods after calcinations at 500°C for 4h. TGA is an important technique to determine the calcination temperature and

thermal stability which can affect the performance of TiO_2 nanoparticles for phenol degradation. Previous studies show that TiO_2 calcined at 400°C is amorphous in nature and had many imperfections and defects, which act as recombination centers for the photo-formed electrons and holes. If the calcinations temperature is increased between 550 to 600°C, TiO_2 anatase phase can be transferred to the rutile phase and led to decrease in degradation [15]. On the basis of this information, the calcination temperature has been selected as 500°C and a well crystalline TiO_2 with anatase was obtained as observed from XRD analysis. There was no weight loss observed after 320°C for TiO_2 synthesized by the hydrothermal method or by the sol-gel method, indicating that the decomposition of the precursor was completed and material is stable at high temperatures. Minor weight loss (2 wt%) before 320°C was attributed to the removal of residual ethanol and water.

3.1.4. Fourier Transform Infra-Red Spectroscopy (FTIR)

The FT-IR spectra of TiO_2 nanoparticles prepared with two different methods were analyzed and are presented in Figure **10**. FT-IR is used to determine the functional groups of TiO_2 nanoparticles and spectra are plotted for % transmittance against wave number (cm^{-1}). The spectra of the oxides TiO_2 (SG) and TiO_2 (HT) were collected in the frequency range of 400-4000 cm^{-1}. In TiO_2 prepared sample, between 3000 to 3600 cm^{-1} a broad band was observed and another peak at 1628cm^{-1} shows stretching and bending vibration of hydroxyl (O-H). A strong absorption peak was observed between 450 and 800 cm^{-1} which was assigned to the Ti-O-Ti stretching and bending bands and attributed to the formation of TiO_2 nanoparticles. Absence of the peak at 2900cm^{-1} shows that all the organic compounds were removed from the samples after calcinations.

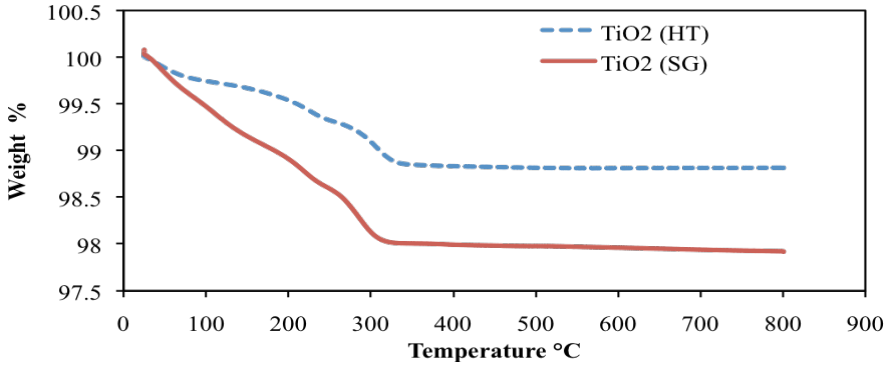

Figure 9: TGA curves of TiO_2 prepared by sol-gel (SG) and hydrothermal (HT) Methods.

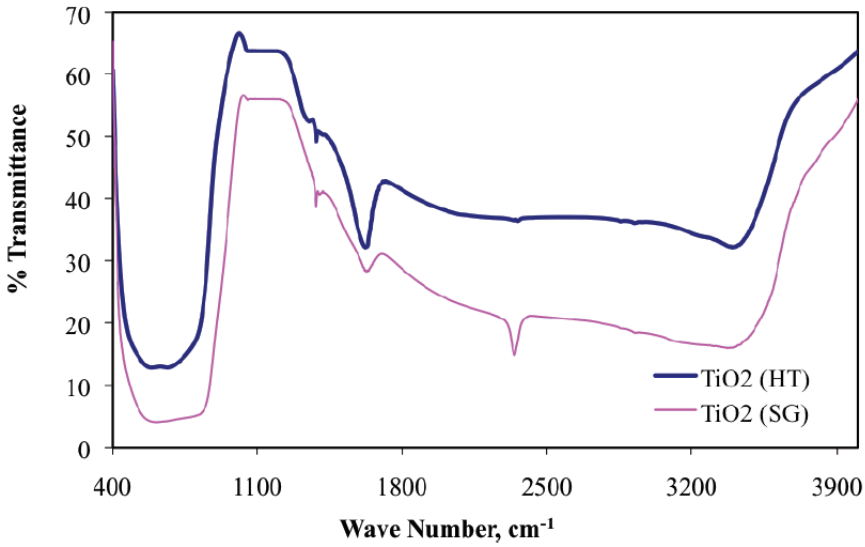

Figure 10: Fourier Transform Infrared Spectra of TiO_2 prepared by sol-gel (SG) and hydrothermal (HT) Methods.

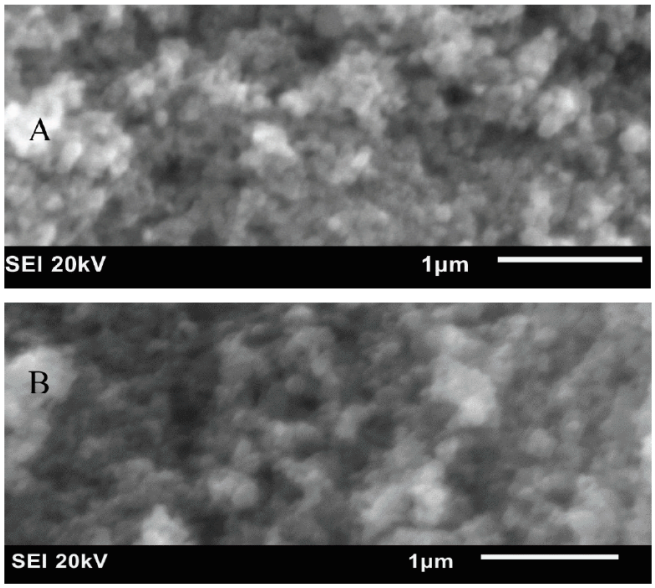

Figure 11: SEM image of TiO_2 nanoparticles prepared by hydrothermal (**A**) and Sol-Gel (**B**) method.

3.2. Morphology of TiO_2 Nanoparticles

Scanning and transmitting electron microscopy was used for determining and differentiating the morphology of materials prepared *via* two different methods. SEM micrographs of the calcined TiO_2 nanoparticles prepared by the sol-gel and hydrothermal methods are shown in Figure **11**(**A**) and **11**(**B**), respectively. The shape of the particles prepared by both methods appears to be spherical however, the particles are fused in TiO_2 (SG) material. Further clarity on particle size and morphology was attained *via* high resolution TEM images (see Figure **12**). It can be seen in Figure **12** that both the materials, TiO_2 (HT) and TiO_2 (SG) have similar particle size and in accordance with the particle size measured by Scherrer's equation. However, it is clear from the TEM images that the material synthesized using sol-gel method has fused surface morphology. This explains the lower surface area shown by catalyst TiO_2 (SG).

3.3. Catalytic Activity of Synthesized TiO_2 Nanoparticles

The catalytic activity of TiO_2 synthesized *via* two different methods was assessed by degrading a 1500 ppm phenol in water solution with two developed treatment systems; microwave and microwave-assisted UV. All experiments were conducted in triplicate.

3.3.1. Dark Adsorption

In a typical dark adsorption experiment, a 300 mL sample containing 1500 ppm phenol in water was mixed with 1.0 g TiO_2 (hydrothermal or sol-gel) in a flask and covered with aluminum foil, and kept for 2 hours in a dark place. This condition was used to understand the significance of microwave irradiation, UV light and TiO_2 on the degradation of phenol. The initial pH of the phenol-water solution was not modified and adsorption of phenol on TiO_2 was assessed. It was observed that phenol degradation did not occur in the dark process, because in the absence of light, photocatalyst (TiO_2) remains inactive and does not produce photo-generated electrons to start the degradation of phenol molecules to occur [17].

3.3.2. Effect of Microwave Radiation on Degradation of Phenol

The effects of microwave irradiation and catalyst prepared by two different methods on degradation of phenol in water was investigated with three processes: (1) MW without addition of catalyst (2) MW-TiO_2 (HT) and (3) MW-TiO_2 (SG).

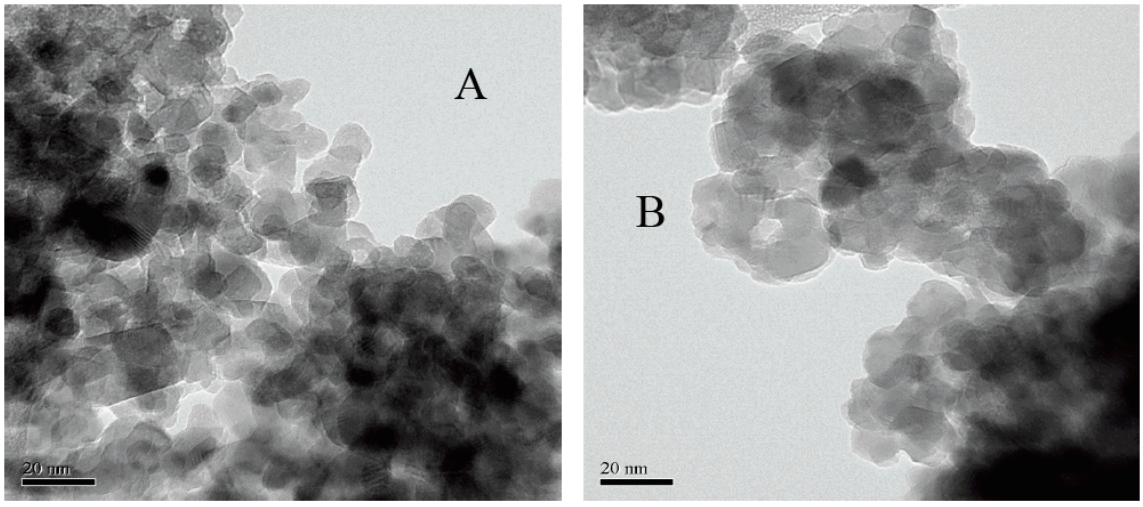

Figure 12: HRTEM image of TiO_2 nanoparticles prepared by hydrothermal (**A**) and Sol-Gel (**B**) method.

The initial phenol concentration was 1500 ppm; volume treated was 300 mL, and catalyst used was 1 g and the reaction time was 120 min. Figure **13** shows the decrease in phenol concentration with microwave irradiation with and without sol-gel and hydrothermal derived TiO_2 nanoparticles. It was observed that microwave irradiation did not have much effect without an oxidant, as the decrease in phenol concentrationn was only 4.47%. Addition of TiO_2 increased the degradation to some extent under microwave irradiation, which might be because microwave irradiation induces a rotation and a migration violently for the motion of polar molecules resulting in the fast increase of the solution temperature due to friction. Additionally, the violent motion of polar substances can lead the molecules to a higher excited state through an increase in collision numbers between reactant molecules, resulting the accelerated rate of phenol degradation [39]. Of the catalysts prepared *via* the two methods, the hydrothermal catalyst showed better catalytic acitivity than did the sol-gel method catalyst by decreasing the phenol concentration to 15.5% as compared to 12.0%. This can be attributed to the large catalyst surface area and pore volume of the catalyst prepared by the hydrothermal method.

3.3.3. Effect of the Microwave Assisted Photocatalytic System on Degradation of Phenol

The effects of microwave radiation combined with UV irradiation on the degradation of phenol were investigated with three processes: (1) MW-UV without catalyst, (2) MW-UV-TiO_2 (HT) and (3) MW-UV-TiO_2 (SG).

The initial phenol concentration was 1500 ppm, the total volume was 300mL with 1 g of catalyst. The energy of MW radiation (E = 0.4-40 kJ mol^{-1} at υ = 1-100 GHz) was considerably lower than that of UV-VIS radiation (E= 600-170 kJ mol^{-1} at λ = 200-700 nm), so it cannot break bonds of common organic molecules [30].

It was found that the microwave-assisted photolytic process exhibited effective decomposition of phenol, with degradation efficiencies of 20.0% for MW-UV-TiO_2 (SG) and 24.0% for MW-UV-TiO_2 (HT) in 120 min, which indicated that the UV light generated by electrodeless lamp could destroy phenol.

The results showed that the catalyst prepared by hydrothermal method had better catalytic activity than that prepared by the sol-gel method. Addition of TiO_2 to the combined MW-UV treatment system resulted in a significant decrease in phenol concentration within 120 min whereas the decrease in phenol concentration with MW-UV only was 7.20%.

On the basis of the above results, microwave-assisted photocatalytic degradation was more effective for the degradation of phenol than any other process studied, perhaps because of direct breaking of bond in phenol by UV irradiation produced. UV irradiation can result in formation of h^+ on the surface of TiO_2 particles,

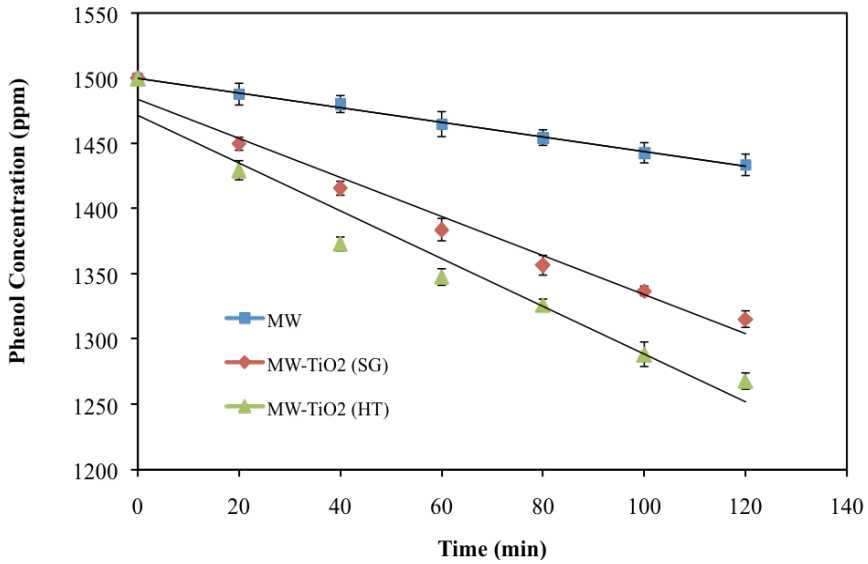

Figure 13: Decrease in phenol initial concentration (1500 ppm) as a function of microwave irradiation at 2.45 GHz with exposure time of 120 min obtained for sol-gel and hydrothermal derived TiO_2 nanoparticles. Error bars represent one standard deviation and may not be visible in some cases due to small values.

which could oxidize phenol. Microwave also creates defective sites on the TiO_2, and the polarization effect of this defective catalyst in a microwave field increases the transition probability of photon-generated electrons and decreases the recombination of e^- and h^+ on the semiconductor surface. Kataoka *et al*. [37] mentioned that under irradiation with combined microwave and UV-VIS light, surface of TiO_2 becomes more hydrophobic, and there is an increase in the hydroxyls on the surface resulting in oxidation to $^{\bullet}OH$. Horikoshi *et al*. [36] proved using electron spin resonance that about 20% more $^{\bullet}OH$ was generated by photocatalysis with microwave irradiation than by photocatalysis alone by electron spin resonance. Figure **14** shows the decrease in phenol concentration in a microwave combined UV irradiation treatment system with TiO_2 nanoparticles.

3.3.4. Effect of Initial Concentration on Phenol Degradation in the MW-UV-TiO_2 Process

Light intensity, dissolved oxygen and initial concentration of the organic substrate are factors on which the reaction rate depends in photocatalytic oxidation of organic pollutants [5, 14].

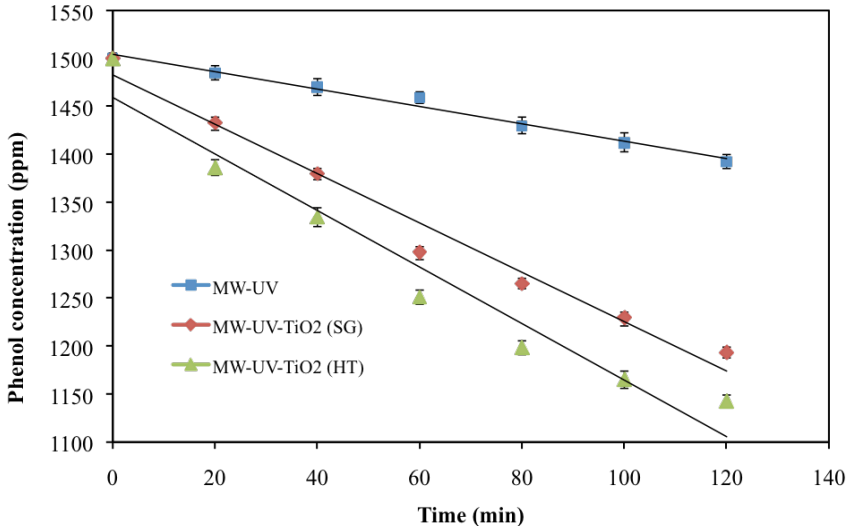

Figure 14: Decrease in initial phenol concentration (1500ppm) as a function of microwave irradiation at 2.45GHz combined UV irradiation exposure time of 120 min obtained for sol-gel and hydrothermal derived TiO_2 nanoparticles. Error bars represent one standard deviation and may not be visible in some cases due to small value.

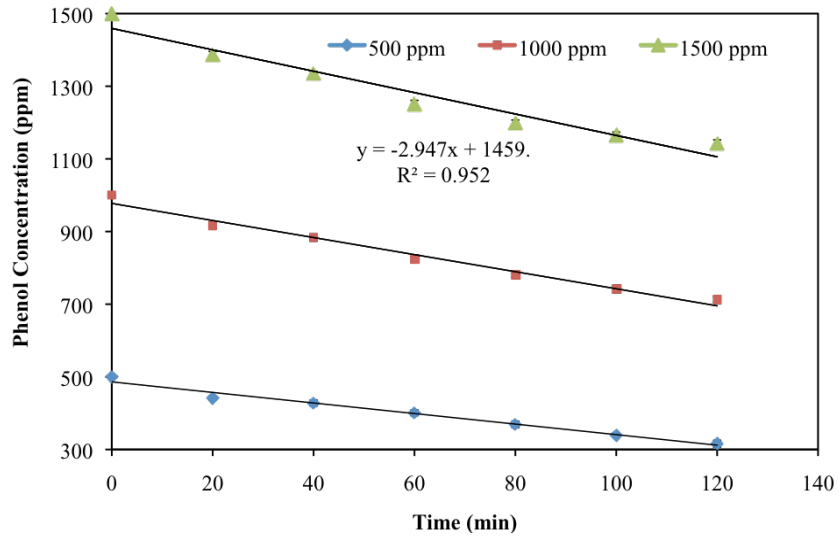

Figure 15: Effect of the initial concentration of phenol on MW-UV-TiO_2 with a microwave at 2.45 GHz, UV at 8 watts and Tio_2 prepared with hydrothermal method for Phenol degradation. Error bars represent one standard deviation and may not be visible in some cases due to small values.

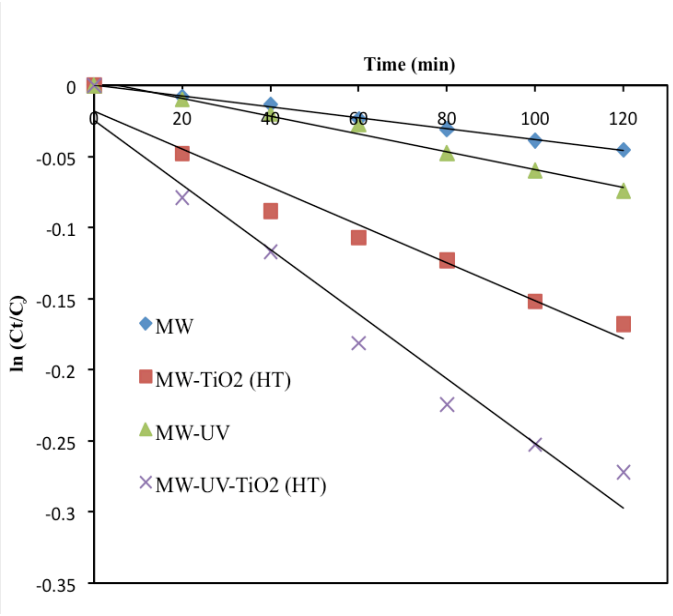

Figure 16: Kinetics of phenol removal at initial concentration 1500ppm.

Previous studies have been done with phenol concentrations above 10 mg/L; in the present study the effect of MW-UV-TiO_2 on phenol degradation was studied using initial concentrations of phenol of 500 ppm, 1000 ppm and 1500 ppm in aqueous solution. The initial pH was 6.9 ± 0.2 without any modification. The catalyst dose and contact time were 1g and 120 minutes respectively. The samples were collected at 20 minute intervals and analyzed for residual phenol concentration. The results obtained are shown in Figure **15**.

The results showed that, the degradation efficiency decreased with an increase in the initial concentration of phenol. The removal percentage of phenol at 120 minutes using the MW-UV-TiO_2 (HT) method was 36.8%, 28.8% and 24.0% for 500 ppm, 1000 ppm and 1500 ppm, respectively. Similar photocatalytic studies have been done by [27, 31], who concluded that with an increase in the initial phenol concentration the rate of photolysis decreased significantly. This could be due to the limited number of active sites on TiO_2.

4. KINETICS OF PHENOL DEGRADATION USING DIFFERENT TREATMENT ALTERNATIVES

The degradation of phenol under MW, MW-TiO_2, MW-UV and MW-UV-TiO_2 with initial concentration of 1500ppm followed a pseudo first order rate equation as a straight line relationship can be seen between logarithmic phenol concentration verses irradiation time [24].

For the first order reaction:

$$Rate = \frac{-\Delta[C]}{\Delta} = K[C] \quad (9)$$

$$= \frac{-d[C]}{dt} = k[C] \quad (10)$$

Integrating the equation (10) and taking ln it can be simplified to equation,

$$\frac{\ln[C]t}{[C]_o} = -kt \quad (11)$$

Figure **16** shows the plot between ln(Ct/Co) and time, which shows the straight line for all the treatment

Table 2: Kinetic Parameter Estimation for Phenol Degradation

Phenol Concentration	Treatment System	Linear Regression Equation	Rate Constant $k \times 10^{-3}$ min^{-1}	R^2 (%)
1500ppm	MW	Y= -0.0004t	0.4	99
	MW-TiO_2 (HT)	Y= -0.0006t	0.6	98
	MW-UV	Y= -0.0013t	1.3	96
	MW-UV-TiO_2 (HT)	Y= -0.0023t	2.3	96

alternatives and slope of each line shows the rate constant for that particular process.

The reaction rate constant (k) for MW-UV-TiO_2 treatment system was found to be 2.3 which shows better reactivity when compared with other alternatives observed in this study. The overall degradation rate decreases in the order of MW-UV-TiO_2 (HT) > MW-UV > MW-TiO_2 (HT)> MW. Generation of OH radical plays an important role for the efficient degradation of phenol under MW-UV-TiO_2 treatment system, UV illuminated TiO_2 might give rise to the generation of additional surface defects and increase in the production of OH radical with an interaction of microwave irradiation. (Table **2**)

CONCLUSIONS

Degradation of phenol in aqueous suspension with TiO_2 was studied under atmospheric pressure. Nanocrystalline TiO_2 catalysts were successfully synthesized using two methods; sol-gel and hydrothermal methods. Then, structure and morphology aspects were characterized using XRD, BET, SEM, HRTEM and FTIR techniques. Two laboratory-scale treatment systems; a microwave treatment system and a microwave-assisted UV irradiation system, were developed to study the degradation of phenol in water. The developed method in this work 'microwave-UV-TiO_2 system' showed the best phenol degradation. The following are the key conclusions: (1) TiO_2 prepared by the hydrothermal method showed better structural, morphological and catalytic activity than TiO_2 prepared by the sol-gel method, (2) Degradation of phenol by microwave-assisted photocatalytic treatment system was more effective than the microwave system alone. Combined method demonstrated the effectiveness and degradation efficiency, (3) The removal of phenol from 300 mL of a 1500 ppm phenol-water solution with 1 g of catalyst was found to be 24.0% with MW-UV-TiO_2 (HT) method, (4) The effect of initial concentration was studied at three concentrations (500 ppm, 1000 ppm and 1500 ppm) with the microwave-assisted photocatalytic system. It was observed that the degradation efficiency decreased with an increase in the initial concentration of phenol, and (5) The removal percentage of phenol at 120 minutes by the MW-UV-TiO_2 (HT) method was 36.8%, 28.8% and 24.0% for 500 ppm, 1000 ppm and 1500 ppm, respectively.

REFERENCE

[1] Patsoura A, Kondarides DI and Verykios XE. Catalysis Today 2007; 124: 94-102. https://doi.org/10.1016/j.cattod.2007.03.028

[2] Rey A, Carbajo J, Adan C, Faraldos M, Bahamonde A. et al. Chemical Engineering Journal 2011; 174: 134-142. https://doi.org/10.1016/j.cej.2011.08.061

[3] Verma Dissertation A. University of Saskatchewan, Saskatoon 2014.

[4] Zhihui A, Peng Y and Xiaohua L. Chemosphere 2005; 60: 824-827. https://doi.org/10.1016/j.chemosphere.2005.04.027

[5] Wang CC, Ying JY. Chemistry of Materials 1999; 11: 3113-3120. https://doi.org/10.1021/cm990180f

[6] Ania CO, Menendez JA, Parra JB and Pis JJ. Carbon 2004; 42: 1383-1387. https://doi.org/10.1016/j.carbon.2004.01.010

[7] Jones DA, Lelyveld TP, Mavrofidis SD, Kingman SW, NJ. Miles, Resources, conservation and recycling 2002; 34: 75-90. https://doi.org/10.1016/S0921-3449(01)00088-X

[8] Muniz EC, Goes MS, Silva JJ, Varela JA, Joanni E, et al. Ceramics International 2011; 37: 1017-1024. https://doi.org/10.1016/j.ceramint.2010.11.014

[9] Granados G, Martinez F and Paez-Mozo EA. Catalysis today 2005; 107: 589-594. https://doi.org/10.1016/j.cattod.2005.07.021

[10] Moussavi G, Mahmoudi M and Barikbin B. Water research 2009; 43: 1295-1302. https://doi.org/10.1016/j.watres.2008.12.026

[11] Senturk HB, Ozdesa D, Gundogdua A, Durana C, Soylakb M, et al. Mater 2009; 172: 353-362.

[12] Huang J, Wang X, Jin Q, Liu Y and Wang Y. Journal of environmental management 2007; 84: 229-236. https://doi.org/10.1016/j.jenvman.2006.05.007

[13] Gully JR. Study of oil sands sludge reclamation under the tailing sludge abandonment research program. Final Report. Canada Centre for Mineral and energy Technology (CANMET), Energy, Mines and Resources Canada, Edmonton, Alta 1992.

[14] Mehrotra K, Yablonsky GS and Ray AK. Industrial and engineering chemistry research 2003; 42: 2273-2281. https://doi.org/10.1021/ie0209881

[15] Porkodi K and Arokiamary SD. Materials Characterization 2007; 58: 495-503. https://doi.org/10.1016/j.matchar.2006.04.019

[16] Barakat MA, Schaeffer H, Hayes G and Ismat-Shah S. Applied Catalysis B: Environmental 2005; 57: 23-30. https://doi.org/10.1016/j.apcatb.2004.10.001

[17] Choquette-Labbe M, Shewa WA, Lalman JA and Shanmugam SR. Water 2014; 6: 1785-1806. https://doi.org/10.3390/w6061785

[18] MacKinnon MD and Sethi A. A comparison of the physical and chemical properties of the tailing ponds at the syncrude and Suncor oil sands plants. In Proceedings of our Petroleum Future Conference, Alberta Oil Sands Technology and Research Authority (AOSTRA), Edmonton, Alta 1993.

[19] Mackinnon MD and Retallack JT. Ann Arbor Science, Denver, Colo 1981; 185-210.

[20] Kavitha M, Gopinathan C and Pandi P. International Journal of Advancements in Research and Technology 2013; 2: 102-108.

[21] Ba-Abbad MM, Kadhum AAH, Mohamad AB, Takriff MS and Sopian K. Int J Electrochem Sci 2012; 7: 4871-4888.

[22] Rehan M, Lai X and Kale GM. Cryst Eng Comm 2011; 13: 3725-3732. https://doi.org/10.1039/c0ce00781a

[23] Vohra MS and Tanaka K. Water Research 2003; 37: 3992-3996. https://doi.org/10.1016/S0043-1354(03)00333-6

[24] Strosher MT and Peake E. Characterization of organic constituents in waters and wastewaters of Athabasca Oil Sands mining area. Report No. 20. Alberta Oil Sands Environmental Research Program (AOSERP), Alberta Environment, Edmonton, Alta 1978.

[25] Hafizah N and Sopyan I. International Journal of Photoenergy 2009.

[26] Allen NS, Edge M, Verran J, Stratton J, Maltby J and Bygott C. Polymer degradation and stability 2008; 93: 1632-1646. https://doi.org/10.1016/j.polymdegradstab.2008.04.015

[27] Kartal OE, Erol M and Oguz H. Chemical engineering and technology 2001; 26: 645-649. https://doi.org/10.1002/1521-4125(200106)24:6<645::AID-CEAT645>3.0.CO;2-L

[28] Klan P, Hajek M and Církva V. Journal of Photochemistry and Photobiology A: Chemistry 2001; 140: 185-189. https://doi.org/10.1016/S1010-6030(01)00422-1

[29] Kumar P. Ph.D. Dissertation, University of Saskatchewan, Saskatoon (2010).

[30] Muller P, Klan P and Cırkva V. Journal of Photochemistry and Photobiology A: Chemistry 2003; 158: 1-5. https://doi.org/10.1016/S1010-6030(03)00101-1

[31] Alnaizy R and Akgerman A. Advances in Environmental Research 2000; 4: 233-244. https://doi.org/10.1016/S1093-0191(00)00024-1

[32] Madill RE, Orzechowski MT, Chen G, Brownlee BG and Bunce NJ. Environ Toxicol 2001; 16: 197-208. https://doi.org/10.1002/tox.1025

[33] Badoga S, Mouli KC, Soni KK, Dalai AK and Adjaye J. Applied Catalysis B: Environmental 2012; 125: 67-84. https://doi.org/10.1016/j.apcatb.2012.05.015

[34] Badoga S, Sharma RV, Dalai AK and Adjaye J. Fuel, 2014; 128: 30-38. https://doi.org/10.1016/j.fuel.2014.02.056

[35] Vilhunen SH and Sillanpaa ME. Journal of hazardous materials 2009; 161: 1530-1534. https://doi.org/10.1016/j.jhazmat.2008.05.010

[36] Horikoshi S, Hidaka H and Serpone N. Journal of Photochemistry and Photobiology A: Chemistry 2004; 16: 221-225. https://doi.org/10.1016/j.nainr.2003.07.003

[37] Kataoka S, Tompkins DT, Zeltner WA and Anderson MA. Journal of photochemistry and photobiology A: Chemistry 2002; 148: 323-330. https://doi.org/10.1016/S1010-6030(02)00059-X

[38] Mishra S. Ph.D. Dissertation, University of Saskatchewan, Saskatoon (2009).

[39] Lai TL, Lai YL, Lee CC, Shu YY and Wang CB. Catalysis Today 2008; 131: 105-110. https://doi.org/10.1016/j.cattod.2007.10.039

[40] Thompson TL and Yates JT. Chemical Reviews 2006; 106: 4428-4453. https://doi.org/10.1021/cr050172k

[41] Chhabra V, Pillai V, Mishra BK, Morrone A and Shah DO. Langmuir 1995; 11: 3307-3311. https://doi.org/10.1021/la00009a007

[42] Rogers VV, Wickstrom M, Liber K and MacKinnon MD. Toxicological Sciences 2002; 66: 347-355. https://doi.org/10.1093/toxsci/66.2.347

[43] Bahnemann W, Muneer M and Haque MM. Catalysis Today 2007; 124: 133-148. https://doi.org/10.1016/j.cattod.2007.03.031

[44] Chen X and Mao SS. Chemical reviews 2007; 107: 2891-2959. https://doi.org/10.1021/cr0500535

[45] Liu X and Yu G. Chemosphere 2006; 63: 228-235. https://doi.org/10.1016/j.chemosphere.2005.08.030

[46] Liu X, Zhang Q, Zhang G and Wang R. Chemosphere 2008; 72: 1655-1658. https://doi.org/10.1016/j.chemosphere.2008.05.030

[47] Bi XY, Peng W, Jiang H, Xu HY, Shi SJ and Huang JL. Journal of Environmental Sciences 2007; 19: 1510-1515. https://doi.org/10.1016/S1001-0742(07)60246-0

[48] Zhang X, Hayward DO, Lee C and Mingos DMP. Applied Catalysis B: Environmental 2001; 33: 137-148. https://doi.org/10.1016/S0926-3373(01)00171-0

[49] Zhang X, Hayward DO and Mingos DMP. Catalysis Letters 2003; 88: 33-38. https://doi.org/10.1023/A:1023530715368

[50] Hsieh YH, Wang KH, Ko RC and Chang CY. Water science and technology 2000; 42: 95-99.

[51] Masuda Y and Kato K. Journal of the Ceramic Society of Japan 2009; 117: 373-376. https://doi.org/10.2109/jcersj2.117.373

[52] Ai Z, Yang P and Lu X. Journal of hazardous materials 2005; 124: 147-152. https://doi.org/10.1016/j.jhazmat.2005.04.027

[53] Gao Z, Shao Gui Y, Sung C and Hong J. Separation and Purification Technology 2007; 58: 24-31. https://doi.org/10.1016/j.seppur.2006.12.020

[54] Levesque CM. MSc Thesis 'Oil sands process water and tailings pond contaminant transport and fate: physical, chemical and biological processes'. University of British Columbia (Vancouver) July 2014.

Received on 22-11-2017 Accepted on 01-12-2017 Published on 21-12-2017

DOI: http://dx.doi.org/10.15377/2410-3624.2017.04.2